Check for updates

Understanding Deviations between Spatially Resolved and Homogenized Cathode Models of Lithium-Ion Batteries

Adrian Schmidt,* Elvedin Ramani, Thomas Carraro, Jochen Joos, André Weber, Marc Kamlah, and Ellen Ivers-Tiffée

Porous electrode models are essential for inexpensively predicting the performance and lifetime of lithium-ion batteries. Physics-based models range from microscopic 3D models, which spatially resolve the microstructural characteristics of all phases in porous electrodes, to reduced and computationally effective models, which do not resolve the microstructure. The homogenized Newman model, also known as the pseudo-2D (P2D) model, is well established and widely used. However, the necessary simplification shows its weaknesses, especially for high charge and discharge rates, and these lead to significant differences in comparison with the microscopic 3D model. Herein, the validity of the homogenized Newman model is investigated with respect to variations of the microstructural characteristics of a porous cathode. The effects of 1) a homogenized conductive additive; 2) non-spherical particle geometries; and 3) overlapping particles on charge/discharge curves are analyzed. The result is a better understanding of the validity limits of P2D models. These new insights about the individual influences of the simplifications will be used to improve the homogenized model. The simulation of complex cathode structures, where several homogenization assumptions are violated, shows that the improved homogenized model reaches a very high accuracy, and, thus, overcomes the existing limitations of the P2D model approach.

1. Introduction

An electrochemical cell from a lithium-ion battery (LIB) consists of two porous electrodes (anode and cathode), which are separated by a porous material (separator). The electrodes store lithium within the crystal structure of the active material and provide it to the liquid or solid electrolyte that acts as a transport path for lithium ions between the two electrodes. The electron transport is provided by the electrodes and the metallic current collectors, which serve as the terminals to an external circuit. Typically, the anode is a two-phase composite, consisting of electrolyte and anode material (e.g., graphite), whereas the cathode can be a three-phase composite consisting of electrolyte, cathode active material (e.g., $LiFePO_4$ and $LiCoO_2$), and electronic conducting additives (e.g., carbon black), all held together by a binder. Alternatively, the cathode can consist of four phases, when a mixture of two different active cathode materials is used ("blend cathode"). This article deals with modeling approaches for simulating a three-phase composite cathode.

Active materials themselves have inadequate electrical conductivities. Therefore, the distribution of carbon/binder phase in the pore space between the active material particles is essential for improving the electronic transport path from the current collector to the active material phase. If part of the active material is not electronically connected, it does not contribute to the capacity of the battery. Both electronic conducting and binder phases are structurally important, and their distribution has an important influence on the cathode performance.[1–3] The distribution of the carbon/binder phase can influence the effective transport properties of both the

A. Schmidt, E. Ramani, Dr. J. Joos, Dr. A. Weber, Prof. E. Ivers-Tiffée
Institute for Applied Materials–Materials for Electrical and Electronic Engineering (IAM-WET)
Karlsruhe Institute of Technology (KIT)
Adenauerring 20b, 76131 Karlsruhe, Germany
E-mail: adrian.schmidt@kit.edu

Prof. T. Carraro
Applied Mathematics
Helmut Schmidt University/University of the Federal Armed Forces Hamburg (HSU/UniBwH)
Holstenhofweg 85, 22043 Hamburg, Germany

Prof. M. Kamlah
Institute for Applied Materials–Materials and Biomechanics (IAM-WBM)
Karlsruhe Institute of Technology (KIT)
Forschungszentrum 696, 76344 Eggenstein-Leopoldshafen, Germany

**ADVANCED
SCIENCE NEWS**

www.advancedsciencenews.com

Energy Technology

Generation, Conversion, Storage, Distribution

www.entechnol.de

electrolyte and of the active material. These effects can be studied microscopically using 3D tomographic reconstructions of the electrodes in combination with 3D modeling approaches. Indeed, tomographic reconstructions of anode and cathode give a perfect picture of their microstructures from a geometric point of view.[4–6] They can also be used to characterize the transport properties of the electrodes.[7–9]

LIB electrode modeling is carried out with different approaches. This work deals with physics-based models that can suitably simulate a battery cathode based on the material properties, the microstructure of the electrode, and the working conditions (e.g., temperature or applied current). A well-known, and widely used, model is the "Newman model" also known as the Doyle–Fuller–Newman model. The development of this model began at the Newman group at Berkeley[10–16] and was also carried out by other groups; e.g., see the previous studies.[17–19] The Newman model is usually associated with its homogenized version, which was first derived by volume averaging in the original work,[10] and then formally by two-scale expansion.[20] In the homogenized version, the model considers cells with the simplification of monodisperse spherical active material particles immersed in an electrolyte solution. It results in a so-called pseudo-2D (P2D) model, where one dimension is the homogenized electrode, and the other dimension is given by the spherical particles of active material. To improve the microstructure modeling in the homogenized model, an extension of the P2D Newman model was developed by Ender, which still describes the active particles as spherical particles, but with a given size distribution.[21]

The Newman model is used extensively in its P2D version, while the full microscopic 3D version has so far been used in very few studies.[22–24] The reason for this is the numerical complexity associated with the solution of the 3D model. The homogenized P2D model is typically assumed to be a good compromise between accuracy and computational costs. Nevertheless, it is not always possible with homogenized models to determine which aspect of the reduced model makes the results inaccurate. When comparing a P2D model with experimental data, it is difficult to determine whether the possible deviations are due to the validity of the homogenized model or to poor parameterization of the model. Therefore, it is essential to investigate the limit of validity of the P2D model. This is done, for example, by Arunachalam et al., where some limits of the homogenization approach are considered, but no comparison between the 3D model and the P2D model is performed.[25]

For example, Taralova et al. showed a comparison between 3D and P2D battery models, but the geometries were simplified, and no carbon/binder phase was considered.[26] The authors showed two cases, both considering a periodic arrangement of active material. In the first test case, the microstructure consisted of overlapping spherical particles. In the second test case, the periodic arrangement consisted of randomly placed, overlapping ellipsoid and spherical particles of different sizes. In the cited work, the agreement between the 3D and P2D models was very good. However, this can only be shown in the unrealistic cases where the carbon/binder phase is disregarded. In fact, the present article shows that a similar comparison, which also includes the carbon/binder phase, reveals large differences between the two model approaches, unless the P2D model is appropriately adjusted. A further comparison between 3D and P2D approaches

is shown by Goldin et al. to improve the P2D model.[22] The 3D models have been used to simulate battery discharge performance as a function of electrode packing configurations and/or discharge rate. The scope was to determine empirical relationships for required parameters of the P2D model. In particular, an effective particle radius was determined as a function of the porosity and the specific surface area of the electrode. This improved the transport process modeling in the active particles, but the carbon/binder phase was disregarded, and the considered microstructures were limited to overlapping spherical active particles.

In a recent work by Hein et al., the important influence of conductive additives and binder on cathode impedance and the role of the electrode morphology are shown, combining 3D microscopic simulations with impedance measurements.[27] While 3D microscopic modeling is appropriate when studying the influence of the carbon/binder phase, a simplified model that can describe these microscopic effects without complex 3D simulations would be preferable and beneficial to the design of new electrodes.

The purpose of this article is to study and improve the validity of homogenized models focusing on the influence of the carbon/binder phase on cell performance. To the best of our knowledge, a quantitative comparison between the 3D and the P2D approach, that also considers a realistic microstructure and the presence of carbon/binder phase, has never been presented in the literature. In this work, a hierarchy of four models will be compared with increasing microscale definition to test different homogenization approaches. For a systematic investigation of the microstructural influence, microstructures with desired, predefined properties are particularly helpful and are here generated by a newly developed virtual microstructure generator.[28] After defining a representative volume element for the 3D models, the simulation results of the three models are compared with each other with different degrees of simplification, which allows conclusions to be drawn about the relevance of homogenization of the conductive additive. Subsequently, the influences of 1) non-spherical particle geometries and 2) overlapping particles on the discharge behavior are analyzed using specially generated microstructures. These new findings on the individual influences of the simplifications are used to improve the homogenized model, so that it can simulate realistic, complex structures with a very high accuracy and, thus, overcome the existing limitations of the P2D model.
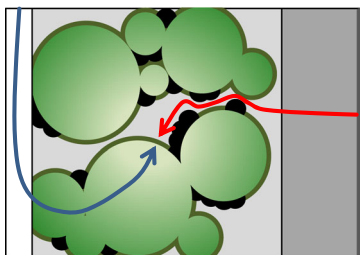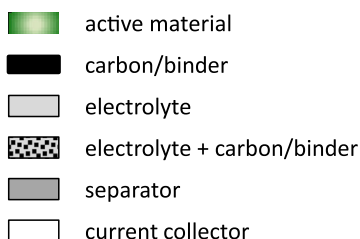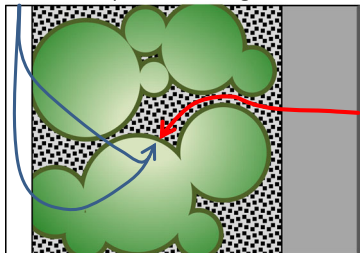
2. Methodology

2.1. Model Description

Figure 1 shows two 3D models and two P2D models considered in this study: 1) a 3D model with separated phases (3D(SP)), in which the electrode is spatially resolved, i.e., the active material phase, the electrolyte, and the carbon/binder phase; 2) a 3D, but partially homogenized model (3D(PH)), in which the active material phase is still spatially resolved, whereas the carbon/binder phase and the electrolyte are treated as one homogeneous phase, filling the pore space with effective ionic and electronic transport properties; 3) the extended homogenized model (EHM), in which the active material phase is a distribution of spherical particles
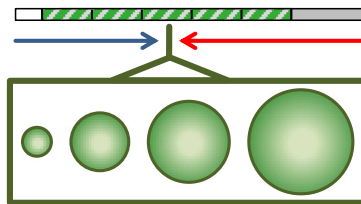
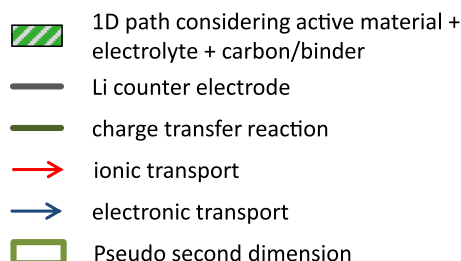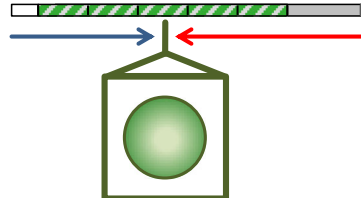**Figure 1.** Schematic illustration of the four models considered here with an exemplary ionic and electronic transport path, coupled by the charge transfer reaction at the particle surface.

with different radii within the porous electrode, which is treated as 1D homogeneous, and 4) the state-of-the-art P2D model, in which the active material phase is considered as one size spherical particles. In this study, all four models are configured as a half-cell of an lithium-nickel-cobalt-aluminum-oxide/ lithium-cobalt-oxide (NCA/LCO) cathode against metallic lithium. The carbon/binder phase is the conductive phase and summarizes the carbon black particles and the binder phase, and the latter is not discussed explicitly. This carbon/binder phase can have an effective electric conductivity up to $650\,\mathrm{S\,m^{-1}}$.[29]

The two 3D model geometries are resampled to a voxel size of 200 nm (voxel = volumetric pixel), preprocessed by island removal operations and meshed with the software Synopsys Simpleware ScanIP. All four models are implemented in COMSOL Multiphysics 5.3 using the Batteries and Fuel Cells module and the Transport of Diluted Species interface. Starting with the model description of the 3D(SP) model including the underlying equations, the stepwise increasing homogenization from the 3D(PH) model to the EHM model toward the P2D model is described as follows.

The 3D(SP) model is based on the Doyle–Fuller–Newman model.[10] It consists of a set of equations that describes transport in the active material phase and in the electrolyte, as extensively explained by Fuller et al. and briefly introduced in the

following.[16] Ionic transport within the electrolyte is modeled using the theory of concentrated solution describing the conservation of mass (Equation (1)) and the current density (Equation (2)) in the electrolyte.

$$\frac{\partial c_l}{\partial t} = \nabla \cdot \left(D_l \nabla c_l - \frac{i_l t_+}{F} \right) \tag{1}$$

$$i_l = -\kappa \nabla \phi_l + \frac{2 \cdot \kappa \cdot R_g \cdot T}{F} \cdot \left(1 + \frac{\partial \ln f}{\partial \ln c_l} \right)(1 - t_+) \nabla \ln c_l \tag{2}$$

Here, c_l represents the lithium concentration in the electrolyte, D_l is the effective diffusion coefficient in the electrolyte, F is the Faraday constant, t_+ is the transference number, i_l is the electrolyte current density, R_g is the universal gas constant, κ is the ionic conductivity, ϕ_l is the potential, and $\frac{\partial \ln f}{\partial \ln c_l}$ is the thermodynamic factor of the electrolyte.

Lithium diffusion in the active material and the electron transport to the charge transfer region is considered by the model. The lithium diffusion results from the concentration gradient and is modeled by Fick's law (Equation (3)). The electronic transport is driven by the electrical potential gradient and is described by the ohmic law (Equation (4)). The electric potential is determined on the domain defined as the unit of active particles and conductive

**ADVANCED
SCIENCE NEWS**
www.advancedsciencenews.com

Energy Technology
Generation, Conversion, Storage, Distribution
www.entechnol.de

additive. The conductive additive has a much higher electrical conductivity σ_s than the active material and is clearly dominating.

$$\frac{\partial c_s}{\partial t} = \nabla \cdot (D_s \nabla c_s) \tag{3}$$

$$i_s = \sigma_s \nabla \phi_s \tag{4}$$

The transport processes in the active material and in the electrolyte are coupled by the charge transfer reaction at their interface, where the lithium ions in the electrolyte react with an electron, form elemental lithium, and intercalate into the active material. The charge transfer current i_{ct} is quantitatively described by the Butler–Volmer kinetic (Equation (5)), with the charge transfer overvoltage η_{ct} (Equation (6)) as the driving force. Furthermore, the charge transfer is ruled by the lithium concentrations in the electrolyte c_l and in the active material c_s. The influence of the active material concentration c_s on the charge transfer is of particular relevance for the interpretation of the results. The contained term $(1 - c_s/c_{s,max})$ approaches 0 for concentrations near 0 as well as for values near $c_{s,max}$, inhibiting the charge transfer process. While chemical instabilities of technically relevant active materials prohibit complete delithiation during charging, the lithium concentration nearly reaches $c_{s,max}$ during discharging and gives rise to a very high charge transfer overvoltage. Hereby, only the lithium concentration on the surface of the active material is decisive. At very high concentration gradients in the active material, the charge transfer reaction ends before the lithium concentration inside the particles reaches a value close to $c_{s,max}$.

$$i_{ct} = F \cdot k \cdot c_l^{\alpha} \cdot c_s^{1-\alpha} \left(1 - \frac{c_s}{c_{s,max}}\right)^{\alpha}$$
$$\cdot \left(\exp\left(\frac{(1-\alpha)F\eta_{ct}}{R_g T}\right) - \exp\left(-\frac{\alpha F \eta_{ct}}{R_g T}\right)\right) \tag{5}$$

$$\eta_{ct} = \phi_s - \phi_l - \phi_{ocv}(c_s) \tag{6}$$

The 3D(PH) model considers carbon/binder phase and electrolyte as a homogenized phase (see Figure 1, bottom left), which has ionic conductivity and electronic conductivity, respectively. The effective conductivity in Equation (9) and (10) is determined according to their respective volume fractions ε (Equation (7) and (8)) and their tortuosity τ. As there is no established method for defining a reference volume and determining the tortuosity of this combined phase in the pore space $\tau_{CB,PH}$, these are approximated by the Bruggeman relation as the functions of porosity.

$$\varepsilon_{l,PH} = \frac{V_l}{V_l + V_{CB}} \tag{7}$$

$$\varepsilon_{CB,PH} = \frac{V_{CB}}{V_l + V_{CB}} \tag{8}$$

$$\kappa_{l,PH} = \frac{\varepsilon_l}{\tau_{l,PH}} \cdot \kappa = \varepsilon_{l,PH}^{1.5} \cdot \kappa \tag{9}$$

$$\sigma_{CB,PH} = \frac{\varepsilon_{CB}}{\tau_{CB,PH}} \cdot \sigma_{CB} = \varepsilon_{CB}^{1.5} \cdot \sigma_{CB} \tag{10}$$

The EHM model was first published in 2015 by Ender.[21] It is based on the P2D model developed by Newman and Tiedemann, but is extended by implementation of a particle size distribution (PSD) instead of equally sized particles.[10] Herein, each particle radius defines a different transport path instead of an averaged transport property. As in all state-of-the-art P2D models, the electrode geometry in the EHM model is homogenized to a 1D path on which Equation (1), (2), and (4) are solved with effective transport parameters defined as in Equation (11)–(13). While the tortuosity of the liquid phase is computed as described in Section 2.4, the tortuosity of the solid phase was not evaluated explicitly, but the effective electrical conductivity σ_{eff} was evaluated empirically with an in-house developed test bench.[30] The lithium-ion intercalation is modeled by solving a 1D diffusion equation with spherical symmetry for each representative electrode particle (Equation (14)) with particle radius R_i. The effective transport parameters and the active particle equation are the following.

$$\sigma_{eff} = \frac{\varepsilon_s}{\tau_s} \cdot \sigma \tag{11}$$

$$\kappa_{eff} = \frac{\varepsilon_l}{\tau_l} \cdot \kappa \tag{12}$$

$$D_{l,eff} = \frac{\varepsilon_l}{\tau_l} \cdot D_l \tag{13}$$

$$\frac{\partial c_{s,i}}{\partial t} = \frac{\partial}{\partial r_i}\left(D_s \frac{\partial c_{s,i}}{\partial r_i}\right) + \frac{2D_s}{r_i}\frac{\partial c_{s,i}}{\partial r_i}, \text{ for } i = 1, \cdots, N \tag{14}$$

$$D_s \cdot \frac{\partial c_{s,i}}{\partial r} = -\frac{A_{spec,i} \cdot R_i}{\varepsilon_{s,i} \cdot 3} \cdot \frac{i_{ct,i}}{F} \tag{15}$$

where N is the number of particle radii.

Equation (14) is defined for each particle radius of the considered PSD. This is of particular relevance for modeling technical cathode structures, which typically consist of active materials owing a PSD. This results in different surface concentrations and consequently different charge transfer current densities $i_{ct,i}$. Here, the Butler–Volmer equation (Equation (5)) applies as well, but is solved individually for each considered particle size R_i. The individual charge transfer current densities $i_{ct,i}$ of each particle define the flux of lithium ions at the outer surface of the particles and, thus, determine the boundary condition for the diffusion equation according to Equation (15). Therein, the flux of lithium ions has to be scaled from the surface-volume ratio of a sphere $(3/R_i)$ to that of the active material (A_{spec}/ε_s).

The total volume specific charge transfer current q_{ct} is determined by the weighted sum of the current densities $i_{ct,i}$ of each effective particle with radius R_i.

$$q_{ct} = A_{spec} \cdot i_{ct} = \sum_i A_{spec,i} \cdot i_{ct,i} \tag{16}$$

The state-of-the-art P2D model is represented by reducing the EHM model to consider only one particle size ($N = 1$).

In that way, a hierarchy of simplifications is achieved from a spatially fully resolved 3D model to a state-of-the-art P2D model. The crucial approximations in the state-of-the-art P2D models are: 1) averaging local fluctuations (e.g., due to

the homogenization of the active particles and of locally distributed conductive additives); 2) monodisperse spherical particles; and 3) no particle–particle interaction, whereas the EHM used here overcomes 2) by considering PSDs.

2.2. Parameterization

The model is parameterized to an NCA/LCO–lithium half-cell, whereby the lithium counter electrode is assumed to be ideal (no reaction overvoltage, $\varphi_{OCV} = 0$ V). **Table 1** shows the parameters for the NCA/LCO blend cathode and of the separator, which was extensively investigated by our research group.[31] The listed parameters without reference were experimentally evaluated using well-established approaches.[9,30–33] The blend cathode is combined to effective material parameters of a single material. In this way, the actual four-phase system can be modeled as a three-phase system. The corresponding open circuit potential φ_{OCV} of the cathode is shown in **Figure 2**. It should be mentioned that the comparative methodology of the models shown here is also transferable to other material systems. Therefore, the particular choice of the parameter set used here is of little influence, provided that 1) all hierarchical models use the same material

Table 1. Electrochemical parameters of the NCA/LCO blend cathode and the microstructure parameters of the separator.

| Parameter	Symbol	Value
Exchange coefficient	k	5.68×10^{-9} m s^{-1}
Maximum lithium concentration	$c_{s,max}$	50 061 mol m^{-3}
Lithium concentration @ state of charge (SOC) 100	$c_{s,initial}$	12 515 mol m^{-3}
Electric conductivity of the active material[38]	σ_{AM}	0.1 S m^{-1}
Electric conductivity of the conductive additive[29]	σ_{CA}	500 S m^{-1}
Electric conductivity of the homogenized electrode[30]	σ_{eff}	10 S m^{-1}
Diffusion coefficient	D_s	5.6×10^{-15} m^2 s^{-1}
Porosity of the separator[a]	ε_{sep}	50%
Tortuosity of the separator[a]	τ_{sep}	1.5

[a]Estimated value.
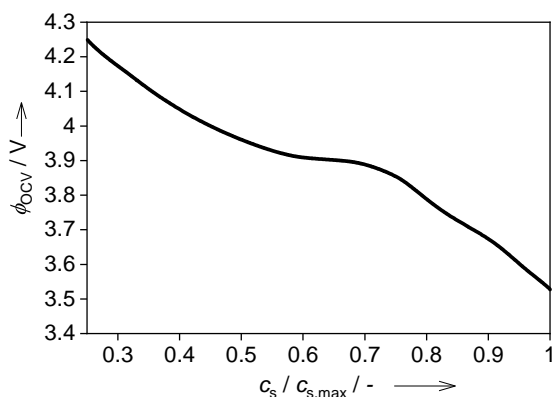
Figure 2. Open circuit potential φ_{OCV} of the simulated NCA/LCO cathode.

parameters, and 2) the parameters are in the right ranges for homogenization and for the electrochemical application under consideration.

The exchange coefficient k given in Table 1 is determined via a transmission line modeling approach, as described by Costard et al.[9] Therein, the macroscopic charge transfer resistance is determined by a fitting procedure of electrochemical impedance measurements to a two-channel transmission line model. This parameter is scaled by the active surface area A_{active} of the electrode, obtained by focused ion beam and scanning electron microscopy (FIB/SEM) tomography, yielding the area specific charge transfer resistance and, finally, the exchange coefficient k of the active material. As the homogenization of the carbon black results in an increased active surface area $A_{active,PH}$, the charge transfer current density is scaled according to the ratio of the specific active areas of the 3D(SP) and 3D(PH) models to obtain the same overall current.

$$i_{ct,PH} = i_{ct} \cdot \frac{A_{active}}{A_{active,PH}} \quad (17)$$

The liquid electrolyte parameters, originally from Nyman et al., are represented in the model by fit functions, as listed in **Table 2** and described by Ender et al.[32,34] Consequently, a LiPF6-based 1 mol L^{-1} electrolyte in an ethylene carbonate and ethyl methyl carbonate (3:7 w:w) solution is modeled.

The four models are compared using the same simulation scenario: The half-cell is discharged with 3C starting from an electrode SOC of 98% until the cutoff voltage of 3.5 V is reached. The temperature is set to a constant value of 298 K.

2.3. Generation of Virtual Microstructures

Microstructure data sets generated by a microstructure model are used in the two 3D models (3D(SP) and 3D(PH)), whereas

Table 2. Electrolyte parameters.

Parameter	Symbol	Value
Conductivity	κ	$\kappa(c_l) = \kappa_{max} \cdot \left(\frac{c_l}{c_{l,\kappa max}} \right) \cdot \exp\left(b(c_l - c_{l,\kappa max})^2 - a \frac{c_l - c_{l,\kappa max}}{c_{l,\kappa max}} \right)$
	κ_{max}	0.984 S m^{-1}
	$c_{l\ \kappa max}$	0.9731 mol L^{-1}
	a	0.85388
	b	-0.162 L^2 mol^{-2}
Diffusion coefficient	D_l	$D_l(c_l) = D_0 + D_1 \cdot c_l + D_2 \cdot c_l^2$
	D_0	4.04×10^{-10} m^2 s^{-1}
	D_1	3.902×10^{-11} m^2 s^{-1} L mol^{-1}
	D_2	-7.280×10^{-11} m^2 s^{-1} L^2 mol^{-2}
Transference number	t_+	$t_+(c_l) = t_{+,0} + t_{+,1} \cdot c_l$
	$t_{+,0}$	0.372
	$t_{+,1}$	-0.06641 L mol^{-1}
Thermodynamic factor	$1 + \frac{\partial \ln f}{\partial \ln c_l}$	$1 + \frac{\partial \ln f}{\partial \ln c_l} = f_0 + f_1 \cdot c_l + f_2 \cdot c_l^2$
	f_0	1.00
	f_1	0.581 L mol^{-1}
	f_2	0.363 L^2 mol^{-2}

**ADVANCED
SCIENCE NEWS**
www.advancedsciencenews.com

Energy Technology
Generation, Conversion, Storage, Distribution
www.entechnol.de

characteristic parameters (porosity and active material fraction, surface area, tortuosity of pore phase, and PSD of active material) are extracted for the two homogenized models (EHM and P2D).[28] The active material particles are assembled by a "dropping and rolling" method, and, in case of the 3D(SP) model only, the conductive phase (carbon black and binder) is stochastically placed between the active material particles.[35] The generation of these microstructures is completely implemented in MATLAB (The MathWorks, Version 2019b, Natik, MA, USA). The method is based on a matrix grid representing the voxel-based microstructure and applies three sequential steps: 1) definition of material portions and PSDs (studies 1–3: either monodisperse spherical or ellipsoidal and study 4: arbitrary-shaped active material particles with a particle distribution mimicked from a "real-life" cathode structure); 2) sequential placement of active material particles in a dimension-specified box; and 3) stochastic placement of carbon/binder agglomerates into the remaining pore space. Each individual carbon/binder agglomerate must overlap with the active material particle above a given threshold, thus ensuring a certain surface coverage. The randomly selected position of the carbon/binder agglomerate is changed until this criterion is met. Thereby, the electrical conductivity is reflected well in the virtual microstructure. This microstructure generation method is newly developed and entirely described by Joos et al. in this issue.[28]

2.4. Microstructure Parameters

The tortuosity τ of the pore phase is calculated by solving the transport equation directly on the 3D geometry.[6] This parameter connects the intrinsic bulk conductivity κ with the effective conductivity κ_{eff} and is applied for the effective conductivity.

The PSD is calculated on the basis of the Euclidean distance transform (EDT).[7] A 3D distance map of the shortest distance to the active material surface results, whose local maxima correspond to the radius of the largest spheres than can be placed inside the particles. These spheres represent the determined PSD, and their radius can be interpreted as the maximum diffusion length inside the particles.

The volume fractions of each phase are calculated in COMSOL Multiphysics by evaluating the individual volume of each phase. The porosity is calculated by simply dividing the volume of the electrolyte phase in the 3D geometry by the sum of the volumes of all phases.

The MacMullin Number is a commonly used parameter to characterize the inhibited transport of a fluid through a porous structure. This number, based on the work of MacMullin and Muccini, relates the intrinsic ionic conductivity of the electrolyte in the cathode to the effective electrolytic conductivity and can be calculated with knowledge of the porosity and the tortuosity according to Equation (18).[36]

$$N_m = \frac{\tau_l}{\varepsilon_l} = \frac{\kappa}{\kappa_{eff}} \qquad (18)$$

The volume-specific active surface area is defined as the surface area between the active material and the pore phase divided by the total volume (sum of all phases). All quantities

are calculated directly in COMSOL Multiphysics based on the tetrahedral mesh.

3. Results and Discussion

This section presents comparative simulation studies of the four models shown in Figure 1. In the first study, the models are compared on the basis of a simple cathode structure with monodisperse spherical particles and small contact areas. In the second study, monodisperse spherical particles with increased contact areas are introduced, thus violating the homogenization requirement. In the third study, a cathode structure with ellipsoidal active material particles is investigated, wherein the ellipsoids are either orientated perpendicular or parallel to the current collector/separator. As the EHM and P2D models are equivalent when simulating monomodal configurations, their results are summarized as EHM/P2D in the first three studies. The new findings about emerging model errors are used to further extend the EHM/P2D models. Thereafter, study 4 introduces a "real-life" cathode with particle shapes from an FIB/SEM reconstruction work, which violates several homogenization assumptions.[28]

The simulations running on the 3D models (3D(SP) and 3D(PH)) were confined to smaller cathode volumes for the sake of computing time. Beforehand, the volume size of a representative volume element is determined (see Supporting Information).

3.1. Study 1: Monodisperse Spherical Particles as Active Material Phase (Small Overlap)

In the first study, the models: 3D(SP), 3D(PH), EHM, and P2D are compared based on a virtual cathode with monodisperse spherical particles of size $r_{3D} = 2.1\mu m$. The overlap between the individual particles is small. The model geometries for the 3D models are shown in **Figure 3** and the corresponding simulation results in **Figure 4**.
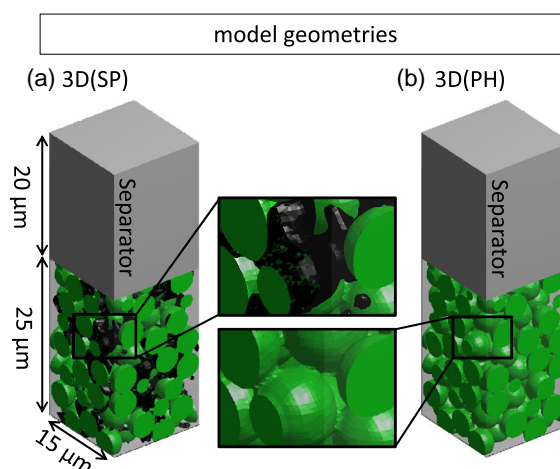

Figure 3. Cathode volume used for the 3D models with monodisperse spherical particles of the a) 3D(SP) model with spatially resolved carbon/binder phase and b) 3D(PH) model with a homogenized carbon/binder and electrolyte phase.
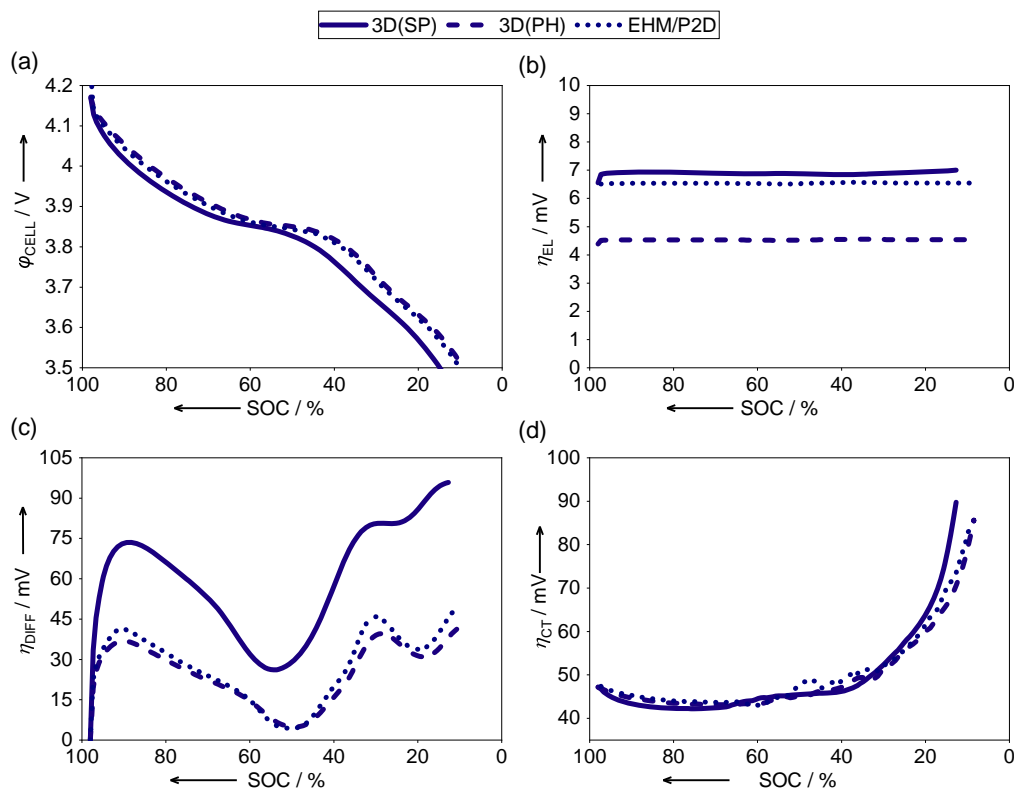
Figure 4. Simulation results of study 1: the active material is represented by monodisperse spherical particles for models 3D(SP), 3D(PH), EHM, and P2D: a) 3C discharge curves, b) electrolyte transport overvoltage η_{EL}, c) solid-state diffusion overvoltage η_{DIFF}, and d) charge transfer overvoltage η_{CT}.

The discharge curves of 3D(PH) coincide with the EHM/P2D models, while 3D(SP) clearly differs, as the voltage over SOC is always lower. The latter is the only one model, which spatially resolves the carbon/binder phase. This result is further examined.

3.1.1. Electrolyte Transport Overvoltage η_{EL}

The electrolyte overvoltage (Figure 4b) of 3D(SP) and EHM/P2D is in good agreement. This indicates that 1) the homogenization of electrolyte transport processes is applicable, and 2) the effective transport parameters are appropriate.[37] In contrary, in the 3D(PH) model, the tortuosity is approximated by the Bruggeman relation as a function of the porosity (see Section 2). In our experience, this approximation always underestimates the tortuosity; thereby, the electrolyte overvoltage is underestimated in the 3D(PH) model as well.[32]

3.1.2. Solid-State Diffusion Overvoltage η_{Diff}

In all of our studies, the solid-state diffusion overvoltage oscillates over SOC, which is due to the course of the equilibrium voltage: According to Equation (S2) and (S3), Supporting Information, the diffusion overvoltage depends on the concentration gradient in the particle and on the gradient of the equilibrium voltage $d\varphi_{OCV}/dc_s$. 3D(PH) and EHM/P2D are well superimposed, whereas 3D(SP) deviates significantly. This effect is caused by the spatially resolved carbon/binder phase, which

covers the surface of the active material particles to a certain extent. Naturally, lithium intercalation is inhibited there, and, as a consequence, the diffusion pathway for lithium is raised. This creates inhomogeneous diffusion pathways and, thus, a higher solid-state diffusion overvoltage. In **Figure 5**, the associated inhomogeneous diffusion in the 3D(SP) model is compared with the 3D(PH) model, wherein the carbon/binder and electrolyte phases are homogenized. For the first time, the interrelation between carbon/binder phase and solid-state diffusion overvoltage is explicitly proved.

3.1.3. Transfer Reaction Overvoltage η_{CT}

The transfer reaction overvoltage is of similar amount and course within all models, as shown in Figure 4d. As described in Section 2, the higher the lithium concentration c_s, the fewer becomes the number of free spaces for lithium intercalation within the crystal structure. This leads to a higher reaction overvoltage at the end of the discharge. The slight deviation of the 3D(SP) model is caused by the partial coverage of the active material particle surface with the carbon/binder phase building up higher c_s gradients, which leads to an increased lithium concentration on the free active surface and, thus, to an earlier inhibition of the charge transfer reaction.

Study 1 demonstrates that the spatial resolution of the carbon/binder phase, only considered in the 3D(SP) model, is indispensable for a correct simulation result. In contrast, the
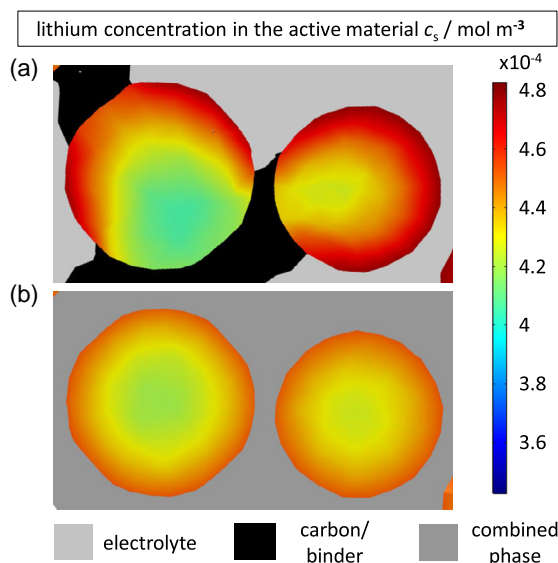
Figure 5. Lithium concentration gradient within two spherical active material particles arising at a 3 C discharge after 975 s simulated for a) the 3D(SP) model with spatially resolved carbon/binder phase and b) the 3D(PH) model with homogenized (carbon/binder and electrolyte) phase.

homogenization of the carbon/binder plus electrolyte phase in the 3D(PH) and EHM/P2D models neglects the effect of inhomogeneous diffusion inside the active material particles. To overcome this weakness of the EHM/P2D model, a diffusion path extension factor (or a larger particle radius) is now empirically introduced. As shown in **Figure 6**, a diffusion path extension factor of 1.5 raises the simulation results of EHM/P2D⟨r⟩ + 50% closer to the 3D(SP) model. The deviation at 3C discharge in Figure 6a is reduced from a maximum of 72 mV to less than 10 mV. However, the η_{diff} curve of the EHM/P2D⟨r⟩ + 50% model in Figure 6b still oscillates, because the proven variation in diffusion length is not included. Therefore, the 3C discharge is simulated again, but now for EHM⟨r⟩ + 50% + PSD with an extension factor of 1.5 plus a PSD, it should be noted that the PSD works as various diffusion paths of different lengths within a single particle. This measure further improves
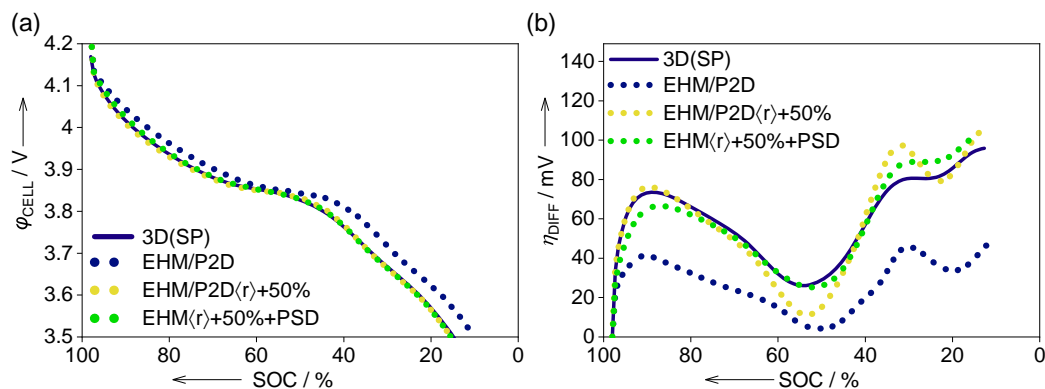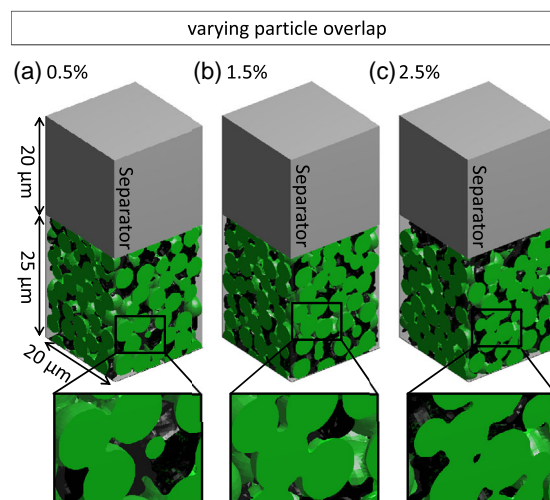

Figure 7. Cathode volume used for the 3D(PH) model with monodisperse spherical particles and a) 0.5%, b) 1.0%, and c) 2.5% overlap of the respective particle volume.

the qualitative agreement between the 3D(SP) and the EHM ⟨r⟩ + 50% + PSD model results, but is not applicable in the state-of-the art P2D model.

3.2. Study 2: Monodisperse Spherical Particles as Active Material Phase (Large Overlap)

Study 2 aims at imitating a cathode structure, which is calendared after tape casting. In this case, most of the active material particles are deformed, and the interparticle contact areas are enlarged. This condition is implemented in the 3D models, but not in the EHM/P2D models, and represents a violation of a homogenization assumption. This study analyses virtual cathode structures with varying degrees of overlapping particles, namely, an overlap of 0.5% (**Figure 7**a), 1.5% (Figure 7b), and 2.5% (Figure 7c) of the respective particle volume. The corresponding microstructure parameters are summarized in **Table 3**. With increasing overlap, active material fractions increase, and a reduced pore space ε_l leads to an increasing

Figure 6. a) 3 C discharge curve and b) solid-state diffusion overvoltage η_{DIFF} of i) the 3D(SP) model, ii) the EHM/P2D model, iii) the EHM/P2D⟨r⟩ + 50% improved using a diffusion path extension factor 1.5, and iv) the EHM⟨r⟩ + 50% + PSD improved using a diffusion path extension factor 1.5 plus a PSD.

Table 3. Microstructure parameters of microstructures with a particle overlap of a) 0.5%, b) 1.0%, and c) 2.5% of the respective particle volume.

Parameter	Respective volumetric overlap of particles		
	a) 0.5%	b) 1.0%	c) 2.5%
ε_{AM} [%]	58.36	63.82	60.74
ε_{EL} [%]	21.45	16.47	17.84
ε_{CB} [%]	20.18	19.81	21.83
A_{spec} [µm^{-1}]	0.373	0.335	0.319
$A_{spec,PH}$ [µm^{-1}]	0.781	0.799	0.733
τ_l [−]	4.429	4.752	6.518
$\tau_{l,PH}$ [−]	1.786	1.898	2.249
N_M [−]	20.65	28.85	36.54
$N_{M,PH}$ [−]	4.29	5.23	5.67
$\langle r \rangle_{EDT}$ [µm]	2.065	2.080	2.066

tortuosity τ_l, whereas the mean particle radii $\langle r \rangle_{EDT}$ determined by the EDT differ only slightly. In the following, the simulation running on the 3D(PH) model is compared with the EHM/P2D models. The 3D(SP) model is not discussed in this case, as we did not want to mix up the influence of particle overlap with the influence of the spatially resolved carbon/binder phase (see study 1).

The simulated discharge curves in **Figure 8**a disclose that the volumetric particle overlap is of significance. At 2.5% overlap, the EHM/P2D differs clearly from the 3D(PH) model. The analysis of the individual loss processes provides more insight.

3.2.1. Electrolyte Transport Overvoltage η_{EL}

It is well known that the available pore space ε_l and its corresponding tortuosity τ_l strongly determine the electrolyte transport. Table 3 lists the according MacMullin numbers, which correlate nicely with the simulated electrolyte overvoltage. It becomes obvious that the approximated tortuosity by the Bruggeman relation in the 3D(PH) causes deviations of more than 20 mV in the electrolyte overpotential.

3.2.2. Solid-State Diffusion Overvoltage η_{Diff}

The solid-state diffusion overvoltage increases slightly with volumetric particle overlap in case of the 3D(PH) model, caused by a declining surface area for lithium intercalation. This increases the diffusion length of lithium atoms in the active material particles, which is not considered in the EHM/P2D models (the EDT algorithm calculates the mean radius only). As a result, the EHM/P2D models do not account for the volumetric particle overlap, which explains the increasing deviation
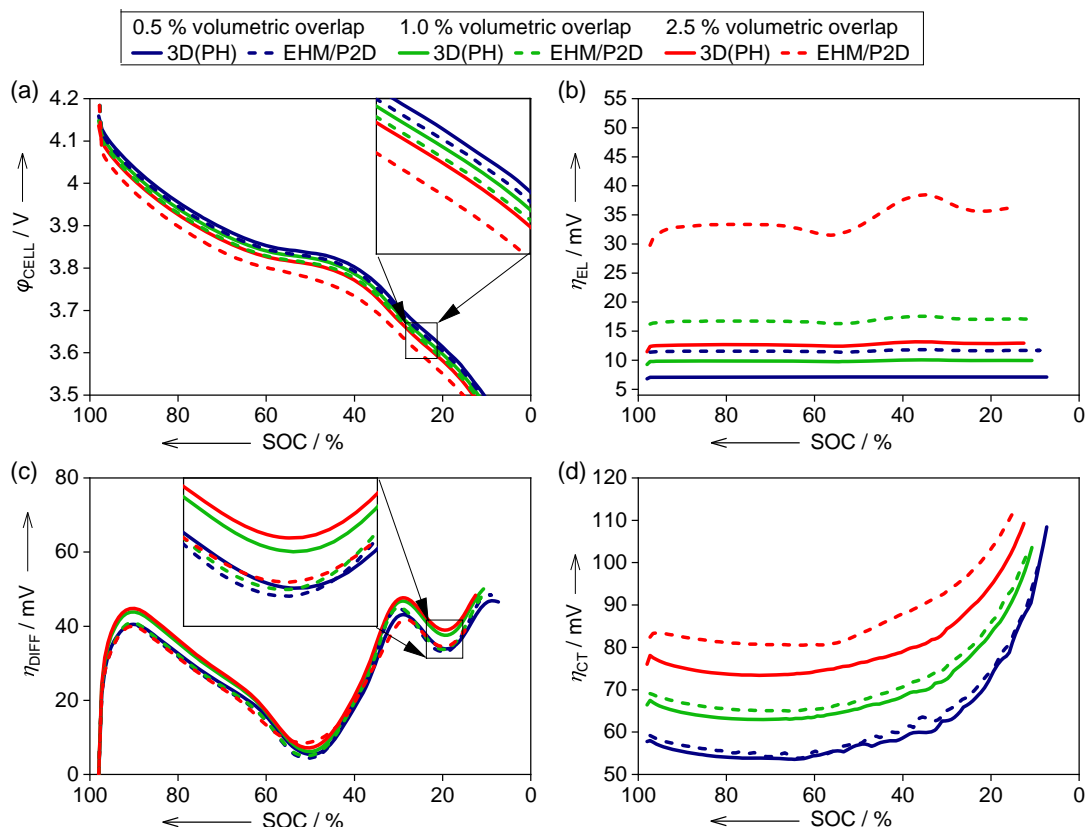

Figure 8. Simulation results of study 2: the active material is represented by monodisperse spherical particles for models 3D(PH) and EHM/P2D with a volumetric particle overlap of 0.5%, 1%, and 2.5%: a) 3C discharge curves, b) electrolyte transport overvoltage η_{EL}, c) solid-state diffusion overvoltage η_{DIFF}, and d) charge transfer overvoltage η_{CT}.

ADVANCED
SCIENCE NEWS
www.advancedsciencenews.com

Energy Technology
Generation, Conversion, Storage, Distribution
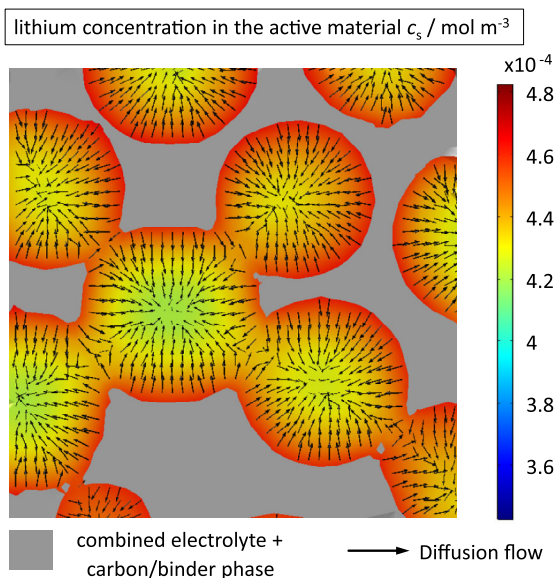www.entechnol.de

Figure 9. Lithium concentration and the diffusion flow of the 3D(PH) model in the spherical active material particles with 2.5% overlap arising at a 3C discharge after 975 s.

Figure 10. Solid-state diffusion overvoltage η_{DIFF} of the 3D(PH) model, the EHM/P2D model, and the empirically improved EHM/P2D$\langle r \rangle + 9\%$ with a diffusion path extension factor of 1.09, all simulated for a 2.5% volumetric particle overlap.

between the EHM/P2D model and the 3D(PH) model. The authors do not expect the direct particle–particle interaction to be the cause for this deviation, because the particles in the 3D model do not seem to exchange a considerable amount of lithium, as shown in **Figure 9**.

3.2.3. Transfer Reaction Overvoltage η_{CT}

The transfer reaction overvoltage increases with increasing volumetric overlap equally for 3D(PH) and EHM/P2D models. This finding is reasonable, as the overlapping active material particles provide less active surface area for lithium intercalation, followed by an increased exchange current density. The EHM/P2D models get the active surface area as a direct input parameter and account for this effect as the 3D(PH) model. The pronounced deviation between the three models at 2.5% volumetric overlap is explained by the influence of electrolyte concentration on the charge transfer reaction: The electrolyte transport in the 3D(PH) model is least inhibited; thus, the concentration gradient is smaller, and thus, the electrolyte depletion is lower. The electrolyte salt concentration is at a value of 780 mol m^{-3} in the EHM/P2D compared with 400 mol m^{-3} in the 3D(PH) model. Due to the term $(c_l)^{\alpha}$ in the Butler–Volmer equation (Equation (5)), electrolyte depletion inhibits the charge transfer process. All in all, the 3D(PH) model underestimates the charge transfer resistance because of a too small tortuosity and electrolyte depletion.

Study 2 demonstrates the effect of an increasing overlap of particles in the cathode structure, which mimics a calendaring process: 1) the reduced pore space causes higher electrolyte overvoltage; 2) the lengthening of the solid-state diffusion paths causes higher diffusion overvoltage; and 3) the reduction of the active surface area causes higher charge transfer overvoltage.
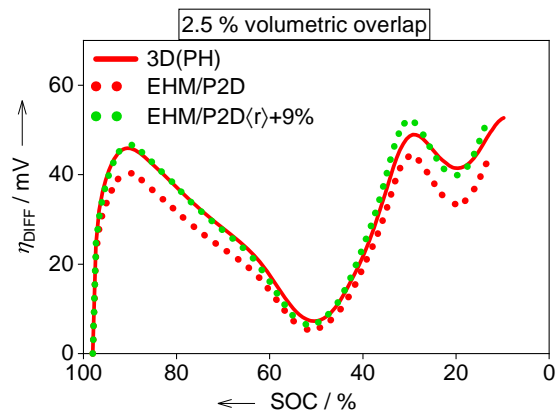
Both 1) and 3) are covered in the EHM/P2D model, provided that the microstructural parameters are correctly determined. Regarding 2), lengthened diffusion paths have to be empirically implemented into the EHM/P2D model. **Figure 10** shows the effect of a diffusion path extension factor of 1.09 introduced in EHM/P2D$\langle r \rangle + 9\%$, reaching far better agreement in solid-state diffusion overvoltage.

3.3. Study 3: Comparison of Spherical and Ellipsoidal Particles as Active Material Phase

This study focuses on a well-known simplification of the P2D model: using monodisperse spherical particles only. This precondition does not consider technical cathode structures, which own particles of different sizes and mostly with a non-spherical shape. Consistently, study 3 investigates structures with ellipsoidal particles. These are generated with an orientation of the largest semi-axis 1) perpendicular to the current collector ($\perp$) and 2) parallel to the current collector ($\parallel$). The larger semi-axis of the ellipsoids is twice as long as the equivalent spherical radius, whereas the other two semi-axes maintain the length $r_{3D} = 2.1\,\mu m$. **Figure 11** shows the corresponding 3D images, wherein the spherical structure is equal to Figure 3a and 5a.

It should be noted that ellipsoids, in general, have a different volume, different half-axis lengths, and a different particle surface compared with spherical particles. To maintain comparability of the structures, we have decided to equate the length of the smallest semi-axis (respective the radius), as the most relevant diffusion length of all particle shapes. Thus, the ellipsoid particles inevitably have a larger volume and a modified specific particle surface. Although the degeneration of spheres generally results in an increased specific particle surface area, the specific particle surface area decreases at the same time as the particle volume increases. The latter effect predominates in our case, so that the ellipsoid microstructures have a lower overall active surface area. **Table 4** lists the microstructural properties of the generated structures. To avoid mixing the influence of

ADVANCED
SCIENCE NEWS
www.advancedsciencenews.com

Energy Technology
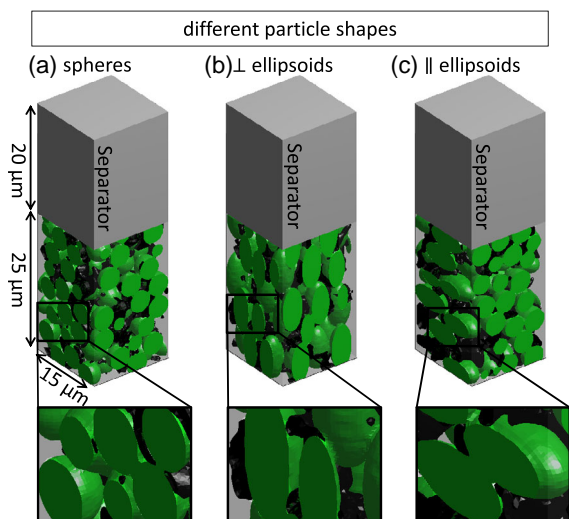Generation, Conversion, Storage, Distribution
www.entechnol.de

Figure 11. Cathode volume used for the 3D(PH) model with different monodisperse particle shapes: a) spherical particles, b) ellipsoids perpendicular to the current collector (⊥), and c) ellipsoids parallel to the current collector (∥).

Table 4. Microstructure parameters of microstructures with spherical particles, ellipsoids perpendicular to the current collector (⊥), and ellipsoids parallel to the current collector (∥).

Parameter	a) Spherical particles	b) ⊥ ellipsoids	c) ∥ ellipsoids
ε_{AM} [%]	49.16	48.87	48.71
ε_{EL} [%]	29.54	30.26	30.68
ε_{CB} [%]	21.26	20.85	20.60
A_{spec} [μm^{-1}]	0.411	0.347	0.346
$A_{spec,PH}$ [μm^{-1}]	0.742	0.626	0.633
τ_l [−]	3.441	2.968	2.090
$\tau_{l,PH}$ [−]	1.621	1.700	1.240
$\langle r \rangle_{EDT}$ [μm]	2.086	2.064	1.982

the particle shape with the influence of the locally resolved conductive additive of the 3D(SP) model (see study 1), the EHM/P2D models are only compared with the 3D(PH) model.

The discharge curves in **Figure 12**a are rather similar for spherical and ellipsoid structures, with only a minor trend to higher overvoltage, most pronounced in the 3D(PH) model. As the analysis of the electrolyte overvoltage only shows the underestimation of electrolyte losses in the 3D(PH) model one more time and, thus, provides no further information, a plot of the cell voltage deviating among the models is inserted instead. The deviation $\varphi_{cath,3D(PH)} - \varphi_{cath,EHM}$ reveals that 1) for spherical structures, the overvoltage in the EHM/P2D model is higher (because the 3D(PH) model underestimates the electrolyte losses, as already discussed earlier) and 2) for ellipsoidal structures, the overvoltage in the EHM/P2D models is lower. The latter simulation result is analyzed in the following.

3.3.1. Solid-State Diffusion Overvoltage η_{Diff}

Despite the same semi-axis length in two spatial diffusion directions in the ellipsoids, the diffusion path along the extended semi-axis gives rise to a higher overvoltage in the 3D(PH) model. In contrast, the diffusion path in the EHM/P2D models is linked to the mean particle radius $\langle r \rangle_{EDT}$. As the EDT considers the smallest half-axis of a particle (see Table 4), the shape variation in this study from spherical to ellipsoidal is obsolete. Therefore, the solid-state diffusion overvoltage in the EHM/P2D models tends to be underestimated.

A 3D illustration of the intercalation current density in ellipsoids, as shown in **Figure 13**, shows its dependency on the length of the half-axis, but not on the electrolyte potential. The assumption that electrolyte concentration or potential gradients along an ellipsoidal particle must result in an inhomogeneous distribution of the charge transfer current density on its surface, even more pronounced for the ellipsoids perpendicular to the current collector, was not confirmed. In conclusion, the intercalation behavior on an ellipsoidal surface seems to depend mainly on the length of the half-axis, but not on the electrolyte potential.

3.3.2. Transfer Reaction Overvoltage η_{CT}

All models calculate a higher transfer reaction overvoltage for the ellipsoid particles, caused by a smaller active surface area and, thus, an increased charge transfer current density. The EHM/P2D model receives the active surface area as a direct input parameter, whereas the 3D(PH) model actively calculates it. Thereby, all models can account for this effect, and the simulated curves are in good agreement.

Study 3 demonstrates that the deviating results between EHM/P2D and 3D(PH) in Figure 12b are 1) 3D(PH) underestimates the electrolyte losses for spherical and ellipsoidal structures, simultaneously causing an underestimation of the corresponding overvoltage and 2) EHM/P2D models underestimate the solid-state diffusion length for ellipsoidal particles, simultaneously causing an underestimation of the diffusion overvoltage. This effect explains a lower total overvoltage in the EHM/P2D model and, thus, a flip of the deviations in Figure 12b from positive to negative values. Furthermore, no significant influence of the orientation of the ellipsoids was observed. For a better agreement between 3D(PH) and EHM/P2D models, we recommend a diffusion path extension factor of 1.15 (EHM/P2D$\langle r \rangle$ + 15%) in the EHM/P2D models. Then, **Figure 14** confirms for perpendicular oriented ellipsoids a far better agreement in solid-state diffusion overvoltage, with a deviation below 5 mV and, therefore, of minor relevance.

In summary, a well-picked diffusion path extension factor for EHM/P2D models can account for elongated diffusion paths originating from carbon/binder phase at the surface of active material particles, from enlarged particle overlap introduced by calendaring or from ellipsoidal particle shapes. In contrast to the P2D model, the EHM model can account for asymmetric diffusion paths within a single particle through a PSD instead of considering monodisperse particles. The effectiveness of our
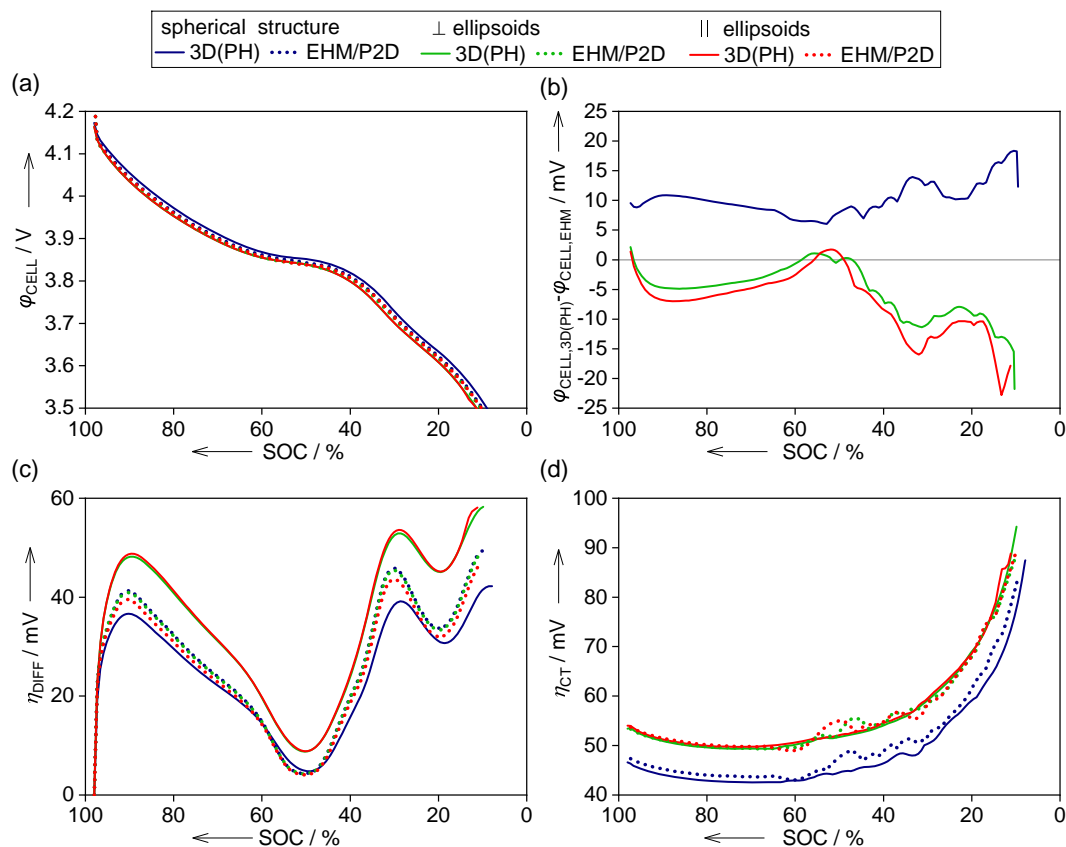
Figure 12. Simulation results for the 3D(PH) and EHM/P2D models using microstructures with spherical particles (blue), ellipsoids perpendicular to the current collector (⊥) (green), and ellipsoids parallel to the current collector (∥) (red): a) 3C discharge curves, b) deviation of the discharge curves $\varphi_{cath,3D(PH)}-\varphi_{cath,EHM}$, c) solid-state diffusion overvoltage η_{Diff}, and d) charge transfer overvoltage η_{CT}.
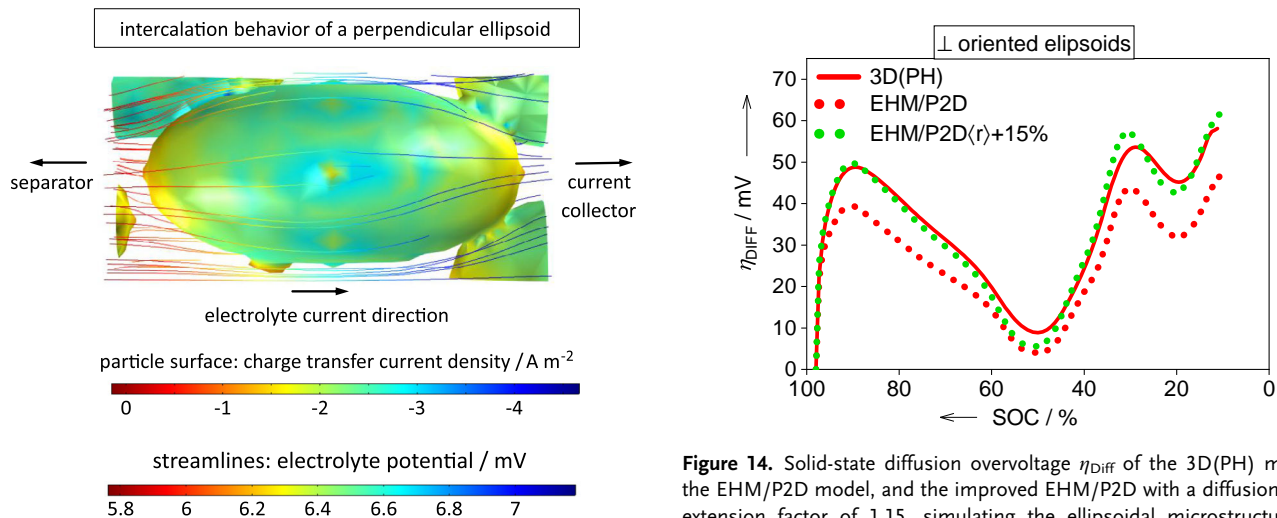

Figure 13. Intercalation behavior on the surface of an ellipsoid perpendicular to the current collector. The surface color of the particle represents the charge transfer current density, and the streamlines are in direction of the electrolyte current and in color of the electrolyte potential.

Figure 14. Solid-state diffusion overvoltage η_{Diff} of the 3D(PH) model, the EHM/P2D model, and the improved EHM/P2D with a diffusion path extension factor of 1.15, simulating the ellipsoidal microstructure in Figure 11b.

3.4. Study 4: A "Real-Life" Cathode Structure

Real-life cathodes violate all of the above-investigated homogenization assumptions at the same time to a large extent. The simulations presented in the following shall disclose, whether the
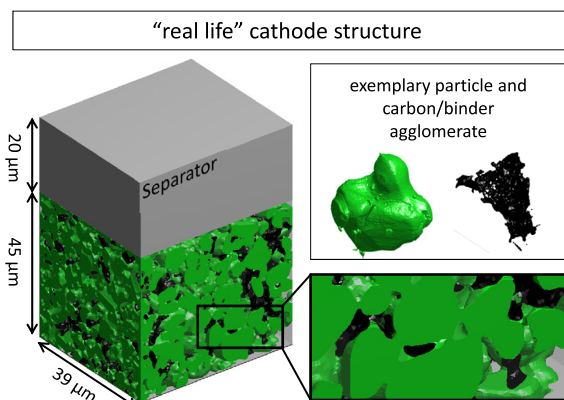
suggestions is proved by modeling a more complex cathode geometry in the following.

Figure 15. A "real-life" but virtual cathode structure with active material particles and carbon/binder phase extracted from a 3D FIB/SEM template and reassembled by a microstructure generator (see Section 2 and Joos et al.)[28]

Table 5. Microstructure parameters of the "real-life" cathode (as shown in Figure 15).

Parameter	ε_{AM} [%]	ε_{EL} [%]	ε_{CB} [%]	A_{spec} [μm^{-1}]	τ_l [−]	$\langle r \rangle_{EDT}$ [μm]
Value	54.29	29.89	15.82	0.46	3.94	2.40

discussed adjustment of the solid-state diffusion length works for such a complex 3D microstructure or not. The microstructure shown in **Figure 15** is created from active material particles and carbon/binder agglomerates by a microstructure generator, as described by Joos et al.[28] The microstructure parameters are listed in **Table 5**, and the simulation results for a 3C discharge are shown in **Figure 16**. The EHM/P2D model was first set up with the mean active material particle size determined by the EDT (configuration 1). Thereafter, two of the above-delivered suggestions for improvement of the homogenized models are introduced: a diffusion path extension factor of 1.4 in EHM/P2D $\langle r \rangle + 40\%$ (configuration 2) and in EHM$\langle r \rangle + 40\%$ + PSD (configuration 3), the strong point of the EHM model, the possible use of a PSD, was activated. Thus, configuration 1) corresponds to the state-of-the-art P2D model, configuration 2) is an improved EHM/P2D setup with a monodisperse particle size, and configuration 3) applies a distribution of active material particle sizes and can be realized with the EHM model only.

The discharge curves in Figure 16a show a significant deviation between the spatially resolved 3D(SP) models, against the homogenized standard EHM/P2D models. But, it becomes obvious that the EHM/P2D$\langle r \rangle + 40\%$ adapts already excellently but seems to deviate a little at SOC > 50%, and the EHM $\langle r \rangle + 40\%$ + PSD model coincides almost perfect with the 3D(SP) model. The use of a diffusion path extension factor by
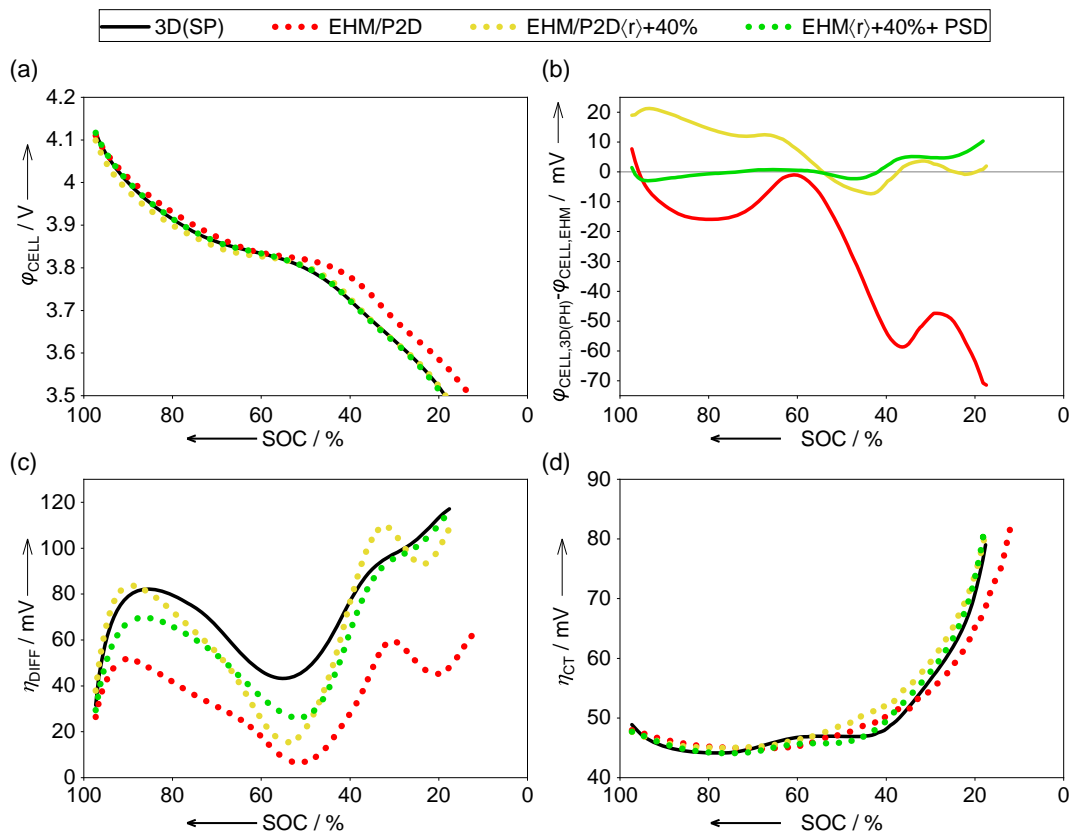

Figure 16. Simulation results of the 3D(SP) running on a high-performance computer, the homogenized EHM/P2D models and the EHM/P2D models simulating a complex 3D cathode microstructure : a) 3C discharge curves, b) deviation of the discharge curves $\varphi_{cath,3D(PH)} - \varphi_{cath,EHM}$, c) solid-state diffusion overvoltage η_{Diff}, and d) charge transfer overvoltage η_{CT}.

**ADVANCED
SCIENCE NEWS**
www.advancedsciencenews.com

Energy Technology
Generation, Conversion, Storage, Distribution
www.entechnol.de

increasing the mean radii in the EHM/P2D$\langle r \rangle$ + 40% elevates the solid-state diffusion overvoltage (Figure 16c) to a similar level as in the 3D(SP) model, improves the course of the charge transfer overvoltage (Figure 16d), and, thus, reduces the maximum deviation in the discharge curves from 77 to 22 mV. Implementing a PSD EHM$\langle r \rangle$ + 40% + PSD accounts for the diffusion paths of different length always existing in "real-life" cathode structures. As a result, the solid-state diffusion overvoltage curve is smoothed and has a better qualitative agreement with the 3D(SP) model. This reduces the maximum deviation in the discharge curves further from 77 mV to less than 10 mV.

4. Conclusion

In this work, homogenized battery-cathode models with different degrees of simplification were investigated and evaluated against each other: 1) a complete microscopic model with separated phases (3D(SP)), in which all phases (the active material phase, the electrolyte, and the carbon/binder) of the electrode are spatially resolved; 2) a partially homogenized model (3D(PH)), in which the active material phase is spatially resolved, while the mixture of carbon/binder phase and electrolyte is treated as a 3D homogeneous phase (distributed in the pore space between the active material particles with effective ionic and electronic transport properties); 3) the EHM, in which the active material is described by a distribution of spherical particles with different radii, and the mixture of electrolyte and carbon/binder phase is treated as 1D homogeneous; and 4) the state-of-the-art P2D model, which further simplifies the active material and only considers particles of a single size.

The EHM model corresponds to the state-of-the-art P2D model (often referred to as the Newman model) when only one particle size is considered. In all models, a 3C discharge process was simulated, and the course of the total cell voltage and the contributions of solid-state diffusion, charge transfer, and electrolyte transport overvoltages were compared.

For the first time, it was shown that the homogenization of the conductive carbon/binder phase causes up to an 85 mV overestimation of the total cell voltage at a 3C discharge. Interestingly enough, this is not an effect of the homogenization of the electrical transport path, but of the reduced active surface area covered by the carbon/binder phase. Even if the charge transfer parameters are adapted to the "true" active surface, solid-state diffusion results in an overvoltage, due to extended diffusion pathways. This is of importance for simulating "real-life" cathode structures with a homogenized model, as these always contain roughly 5–15 vol% carbon/binder phase.

In summary, the state-of-the-art P2D Newman model does not perform well for high discharge rates and "real-life" cathode structures (this criticism holds more or less true for the EHM model). The studies shown here provide helpful advice on how to adapt these models and achieve better approximation accuracy. These allow simulating the complete 3C discharge curve with an accuracy of 10 mV for the EHM and of 22 mV for the P2D model, requiring 14 and 5 s, respectively, on a standard laptop computer. The microscopic 3D(SP) model needs 14 h and 171 GB random access memory on a high-performance computer. Homogenized models are much more convenient for simulating electrodes under different conditions. However, characteristic microstructure parameters are indispensable. While effective transport coefficients of the pore space are calculable by established methods, determining the effective diffusion length is a challenge. For this purpose, the next step is an automated procedure that considers the "true" particle shape and the "free" reaction surface area.

Supporting Information

Supporting Information is available from the Wiley Online Library or from the author.

Conflict of Interest

The authors declare no conflict of interest.

[1] L. Fransson, T. Eriksson, K. Edström, T. Gustafsson, J. O. Thomas, *J. Power Sources* **2001**, *101*, 1.

[2] R. Dominko, M. Gaberšček, J. Drofenik, M. Bele, J. Jamnik, *Electrochim. Acta* **2003**, *48*, 3709.

[3] J. K. Mayer, L. Almar, E. Asylbekov, W. Haselrieder, A. Kwade, A. Weber, H. Nirschl, *Energy Technol.* **2020**, *8*, 1900161.

[4] M. Ender, J. Joos, T. Carraro, E. Ivers-Tiffée, *Electrochem. Commun.* **2011**, *13*, 166.

[5] J. R. Wilson, J. S. Cronin, S. A. Barnett, S. J. Harris, *J. Power Sources* **2011**, *196*, 3443.

[6] M. Ender, J. Joos, A. Weber, E. Ivers-Tiffée, *J. Power Sources* **2014**, *269*, 912.

[7] M. Ender, J. Joos, T. Carraro, E. Ivers-Tiffee, *J. Electrochem. Soc.* **2012**, *159*, A972.

[8] L. Almar, J. Joos, A. Weber, E. Ivers-Tiffée, *J. Power Sources* **2019**, *427*, 1.

[9] J. Costard, J. Joos, A. Schmidt, E. Ivers-Tiffée, *Energy Technol.* **2020**, https://doi.org/10.1002/ente.202000866.

[10] J. Newman, W. Tiedemann, *AIChE J.* **1975**, *21*, 25.

[11] M. Doyle, *J. Electrochem. Soc.* **1993**, *140*, 1526.

[12] M. Doyle, J. Newman, A. S. Gozdz, C. N. Schmutz, J. Tarascon, *J. Electrochem. Soc.* **1996**, *143*, 1890.

**ADVANCED
SCIENCE NEWS**

www.advancedsciencenews.com

Energy Technology
Generation, Conversion, Storage, Distribution

www.entechnol.de

[13] M. Doyle, J. Newman, *J. Appl. Electrochem.* **1997**, *27*, 846.

[14] P. Arora, R. E. White, M. Doyle, *J. Electrochem. Soc.* **1998**, *145*, 3647.

[15] M. Doyle, J. P. Meyers, J. Newman, *J. Electrochem. Soc.* **2000**, *147*, 99.

[16] T. F. Fuller, M. Doyle, J. Newman, *J. Electrochem. Soc.* **1994**, *141*, 1.

[17] P. M. Gomadam, J. W. Weidner, R. A. Dougal, R. E. White, *J. Power Sources* **2002**, *110*, 267.

[18] P. Ramadass, B. Haran, R. White, B. N. Popov, *J. Power Sources* **2003**, *123*, 230.

[19] G. G. Botte, V. R. Subramanian, R. E. White, *Electrochim. Acta* **2000**, *45*, 2595.

[20] F. Ciucci, W. Lai, *Transp. Porous Media* **2011**, *88*, 249.

[21] M. Ender, *J. Power Sources* **2015**, *282*, 572.

[22] G. M. Goldin, A. M. Colclasure, A. H. Wiedemann, R. J. Kee, *Electrochim. Acta* **2012**, *64*, 118.

[23] T. Hutzenlaub, S. Thiele, N. Paust, R. Spotnitz, R. Zengerle, C. Walchshofer, *Electrochim. Acta*, **2014**, *115*, 131.

[24] A. H. Wiedemann, G. M. Goldin, S. A. Barnett, H. Zhu, R. J. Kee, *Electrochim. Acta* **2013**, *88*, 580.

[25] H. Arunachalam, S. Onori, I. Battiato, *J. Electrochem. Soc.* **2015**, *162*, A1940.

[26] V. Taralova, O. Iliev, Y. Efendiev, *J. Eng. Math.* **2016**, *101*, 1.

[27] S. Hein, T. Danner, D. Westhoff, B. Prifling, R. Scurtu, L. Kremer, A. Hoffmann, A. Hilger, M. Osenberg, I. Manke, M. Wohlfahrt-Mehrens, V. Schmidt, A. Latz, *J. Electrochem. Soc.* **2020**, *167*, 013546.

[28] J. Joos, A. Buchele, A. Schmidt, A. Weber, E. Ivers-Tiffée, *Energy Technol.* **2020**, https://doi.org/10.1002/ente.202000891.

[29] G. Liu, H. Zheng, X. Song, V. S. Battaglia, *J. Electrochem. Soc.* **2012**, *159*, 214.

[30] M. Ender, A. Weber, E. Ivers-Tiffée, *Electrochem. Commun.* **2013**, *34*, 130.

[31] M. Weiss, PhD thesis, KIT (Karlsruhe), **2020**.

[32] M. Ender, PhD thesis, KIT (Karlsruhe), **2014**.

[33] J. Schmalstieg, C. Rahe, M. Ecker, D. U. Sauer, *J. Electrochem. Soc.* **2018**, *165*, A3799.

[34] A. Nyman, M. Behm, G. Lindbergh, *Electrochim. Acta* **2008**, *53*, 6356.

[35] Y. Shi, Y. Zhang, *Appl. Phys. A: Mater. Sci. Process.* **2008**, *92*, 621.

[36] R. B. MacMullin, G. A. Muccini, *AIChE J.* **1956**, *2*, 393.

[37] J. Joos, T. Carraro, A. Weber, E. Ivers-Tiffée, *J. Power Sources* **2011**, *196*, 7302.

[38] M. Nishizawa, S. Yamamura, T. Itoh, I. Uchida, *Chem. Commun.* **1998**, 1631, https://doi.org/10.1039/A802962H.

2000881 (15 of 15)